Progress In Electromagnetics Research C, Vol. 134, 249–261, 2023

Design of Three-Band Two-Port MIMO Antenna for 5G and Future 6G Applications Based on Fence-Shaped Decoupling Structure

Zhonggen Wang[1], Wanying Ren[1, *], Wenyan Nie[2], Weidong Mu[1], and Chenlu Li[3]

Abstract—In this paper, a new design of a highly isolated tri-band antenna for 5G and future 6G applications is proposed. The overall dimensions of the proposed antenna are just $56.4 \times 36.6\,\text{mm}^2$; moreover, it contains two monopole antenna units and a defective ground. The tri-band characteristics of the antenna are achieved by improving the single antenna patch structure. The structure is improved based on the original T-shaped decoupling structure to create a fence-shaped decoupling structure consisting of an improved T-shaped and an improved rectangular structure. This will greatly improve isolation by efficiently absorbing the coupling current. Therefore, the proposed antenna system is designed and tested to reach the 5G dual bands of 3.38 GHz–3.61 GHz, 4.51 GHz–4.96 GHz, and the future 6G band of 6.06 GHz–7.51 GHz. The results show that, relative to other antennas, this antenna has an isolation degree in the operating band greater than 13.1 dB. In addition, the antenna has good radiation characteristics and an acceptable envelope correlation coefficient.

1. INTRODUCTION

Since Multiple-Input-Multiple-Output (MIMO) technology can make full use of space resources without increasing the spectrum resources or transmitting the antenna power, exponentially increasing the system channel capacity, and improving the communication quality, it is progressively becoming a key technology in antenna designs [1]. Therefore, multi-band antennas, which enable several communication modes and are crucial technological tools driving the current era's rapid development of wireless communication systems, are among the MIMO antennas that are mostly employed in wireless communication systems. Moreover, several MIMO antennas have been proposed which support various frequency bands [2–22]. For instance, a flawed ground plane-based planar antenna for WiFi/WiMAX/WLAN applications which operates at frequencies of 2.47 GHz, 3.55 GHz, and 5.55 GHz has already been published [2]. In the literature, a brand-new metamaterial-based antenna that acts as a complementary split ring resonator (CSRR) antenna was also introduced [3], where three bands — 1.9 GHz (1.78–1.91 GHz), 2.45 GHz (2.23–2.52 GHz), and 3.2 GHz (2.9–3.25 GHz) — can be covered by the optimized antenna. A compact monopole antenna with a pentagon-shaped patch, symmetrical hook-shaped resonators, and one vertical slot was already described with the claim that it could be used for many communication modes and could operate at three frequencies (e.g., 3.5 GHz, 5.4 GHz, and 8 GHz). It was found that the antenna was useful for Bluetooth, WLAN, and WiMAX applications [4]. Furthermore, a microstrip patch antenna with a hexagon shape was also demonstrated to support more modes [5]. This antenna could operate on three frequencies (e.g., 5.40 GHz, 6.76 GHz, and 8.82 GHz) and was suitable for WLAN, WiMAX (5250–5850 MHz), IEEE 802.11a (5.47–5.725 GHz), 5G unlicensed band (5.2–5.7 GHz), weather monitoring, and radar applications.

Received 15 May 2023, Accepted 30 June 2023, Scheduled 16 July 2023

* Corresponding author: Wanying Ren (1311212462@qq.com).

[1] School of Electrical and Information Engineering, Anhui University of Science and Technology, Huainan 232001, China. [2] School of Mechanical and Electrical Engineering, Huainan Normal University, Huainan 232001, China. [3] School Electrical and Information Engineering, Hefei Normal University, Hefei 230061, China.

However, in miniaturized MIMO antenna devices, due to the near-field radiation and current flow, there will be a severe coupling between antenna elements, which will affect the operating performance of such an antenna. To be compatible with modern portable small communication devices and improve isolation, several methods have been proposed, including loading ground branches using defective ground structure (DGS), neutralization line (NL), electromagnetic band gap (EBG), decoupling networks, and other methods. Moreover, Du et al. reported an antenna consisting of two radiating patches placed side by side and a neutralization line, which was inserted between the two patches to achieve decoupling and increase the isolation to 16.3 dB [6]. In addition, Iqbal et al. designed an antenna that consisted of two microstrip line-fed monopoles. F-shaped branches were loaded between the antenna units to produce multiple resonances and high isolation between the radiating elements, whereas the isolation of the antenna was greater than 20 dB [7]. According to [8], two antenna units were symmetrically placed on an FR4 dielectric substrate of size 19 mm × 30 mm to obtain a notched band between 4.37 and 5.95 GHz. Thus, the antenna element was modified to include a T-shaped stub and a sickle-shaped open-ended half-guided-wavelength resonator slot. To create the 6.52–7.42 GHz notch band, a second open-ended half-guided-wavelength resonator slot was added along the lower edge of the radiating patch, and the isolation of the antenna was greater than 18 dB. Furthermore, Masoodi et al. proposed an antenna in which an I-shaped ground structure was used to achieve an isolation of 18 dB while having a size of 40 mm × 29 mm [9]. As for [10], an inverted F-type dual-band MIMO antenna was designed to cover the range between 2.4 GHz and 5 GHz Wireless Local Area Network (WLAN) bands with 15 dB isolation by setting up meandering resonant branches and etching inverted T-slots on the antenna grounding plate. Moreover, in [11], the low mutual coupling between the radiating units was achieved by adding a coupling gap in the defective ground plate, providing better than −13 dB mutual coupling over the entire antenna bandwidth. Furthermore, Tan et al. reported an antenna, and an electromagnetic bandgap structure was inserted between the two radiating units to improve the antenna isolation to −26 dB and −44 dB at 3.48 GHz and 4.88 GHz, respectively [12]. Finally, in [13], the use of open-loop ring resonators not only reduced the size of the antenna element but also provided positive cross-coupling, enabling isolation better than −15 dB and coverage of multiple frequency bands.

To sum up, this work demonstrates a novel structure for a dual-port tri-band MIMO antenna that contains two symmetrical torch-shaped radiating elements with a fence-shaped structure. The fence-shaped branches of the modified ground structure are deployed to achieve a high level of isolation by effectively absorbing currents and lowering the mutual coupling between the two radiating elements. The branches of the modified ground structure are used to generate multiple frequencies to broaden the frequency band by improving the resonance modes. The isolation of the antenna achieves a value greater than 13 dB in all three frequency bands. At the same time, the MIMO antenna also has good radiation and diversity performance.

2. ANTENNA DESIGN

2.1. Antenna Model

Figure 1 illustrates the antenna's geometry. It is printed on a Rogers RO4003 dielectric substrate with a total dimension of 56.4 mm (length), 36.6 mm (width), and 1.524 mm (height), a relative permittivity of 3.55, and a loss tangency of 0.0027. The antenna unit is fed by a microstrip line. The front part of the substrate is a wrench-shaped circular radiation patch symmetrically placed, where each radiation patch consists of a circular radiation patch with a ring, an X-shaped microstrip line, and two mirror-symmetric L-shaped branches. Moreover, the antenna's back part is a metal ground. Among them, the T-shaped branch is directly connected to the ground; three I-shaped slit structures are loaded on the T-shaped branch; and two pairs of symmetrical small rectangles are applied to both sides of the T-shaped branch. In addition, the rectangular part of the ground is hollowed out; the L-shaped branch is added for the operation; and the two antenna elements are placed between each other in a symmetrical form to constitute a fence-shaped structure. Table 1 shows the optimized parametric dimensions of the proposed MIMO antenna.

The antenna's low-resonance mode is generated by a circular radiating patch. In addition, the high resonance is activated by loading two L-shaped antenna branches. These two resonant frequencies are independently adjustable, making the design more flexible. Moreover, the additional L-shaped branches

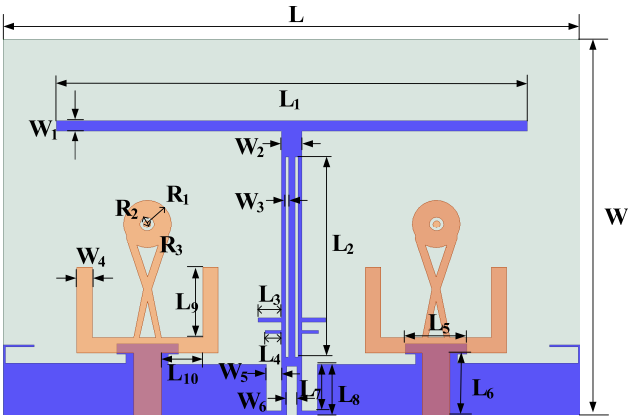

Figure 1. Geometrical structure of the proposed two-port MIMO antenna.

Table 1. Optimized parametric dimensions of proposed MIMO antenna.

Parameters	L	L_1	L_2	L_3	L_4	L_5	L_6	L_7	L_8	L_9	L_{10}
Value (mm)	56.4	46	19.5	2.3	1.6	6	6.1	4.5	5	6.8	4.05
Parameters	W	W_1	W_2	W_3	W_4	W_5	W_6	R_1	R_2	R_3	
Value (mm)	36.6	1	2	0.3	1.5	1.5	1	2.32	0.7	0.35	

on the back of the antenna and the excavation on both sides of the T-shape make the antenna adaptable to future 6G communications.

Figure 2 shows the equivalent circuit of the proposed antenna, where circuit 1 and circuit 3 are equivalent to the wrench-shaped circular radiation patch, and circuit 2 is equivalent to the fence-shaped back panel structure. A circular radiation patch generated a 3.4 GHz band equivalent circuit for R_1, L_1, and C_1 composed of a parallel resonant circuit, and an L-shaped branch generated a 4.9 GHz band equivalent for R_2, L_2, and C_2 composed of a parallel resonant circuit.

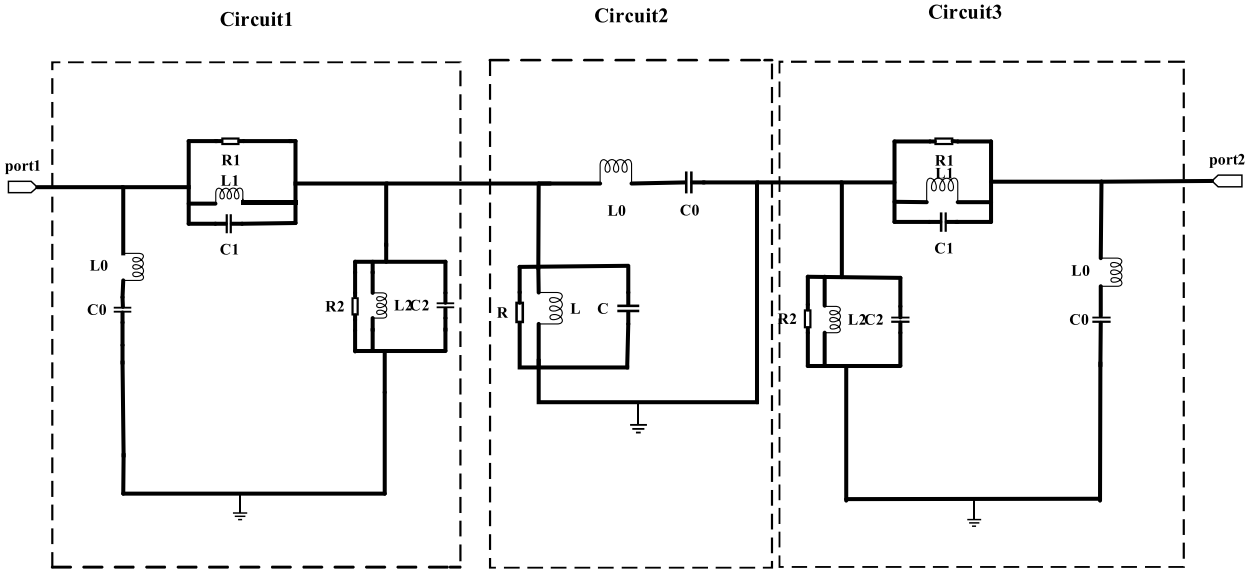

Figure 2. Equivalent circuit of the proposed two-port MIMO antenna.

2.2. Antenna Structure Design Analysis

2.2.1. Antenna Structure Design

The evolution of the antenna structure is shown in Fig. 3. Referring to Fig. 3(a), the design combines a circle and an L-shaped branch to build the basic radiation element. First, a basic radiation unit consisting of a circular radiation patch is designed. The radius of the circular patch (R) can be derived from the following formula [23]:

$$F = \frac{8.791 \times 10^9}{f_{s1}\sqrt{\varepsilon_\gamma}} \tag{1}$$

$$R = \frac{F}{\left\{1 + \frac{2h}{\pi F \varepsilon_\gamma}\left[\ln\left(\frac{\pi F}{2\pi}\right) + 1.7726\right]\right\}^{\frac{1}{2}}} \tag{2}$$

where f_{s1} is the target resonant frequency of the low frequency, h the thickness of the dielectric substrate, and ε_r the relative permittivity. Since the basic radiating element can only exhibit broadband characteristics in a specific frequency range and cannot provide multi-frequency coverage, it seems necessary to change the structure of the antenna patch to achieve this function. In order to achieve multiple frequencies and improve the impedance matching quality of the antenna, symmetric L-shaped branches are added on both sides of the circular patch. The length and resonant frequency of the L-shaped branches can be calculated by the following equation:

$$L_{s2} = L_9 + L_{10} \tag{3}$$

$$f_{s2} = \frac{c}{4L_{s2}\sqrt{\varepsilon_{\gamma eff}}} \tag{4}$$

where $\varepsilon_{\gamma eff}$ is half of the dielectric constant of the Rogers RO4003, L_{s2} the effective length of the L-shaped branch, f_{s2} the second resonant frequency, and c the electromagnetic wave propagation speed. By calculation, the resonant frequency f_{s2} is 4.9 GHz.

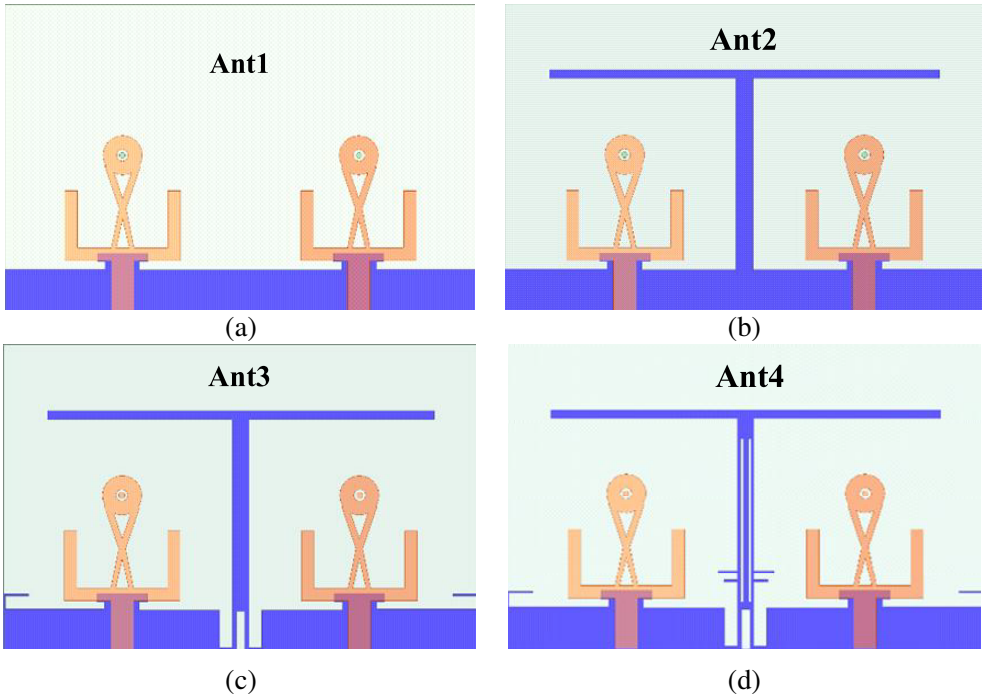

Figure 3. The design evolution of the antenna structure (a) Ant1, (b) Ant2, (c) Ant3, and (d) Ant4.

A rectangular ground plane is printed on the back side of the substrate, whereas two symmetrical torch-type radiation patches are printed on the front side of the substrate, generating resonant frequencies of 3.3 and 6.0 GHz.

As shown in Fig. 3(b), to improve the isolation of the antenna, T-branches are added to the backplane part of the substrate to generate additional coupling paths. Its excitation-side antenna unit couples the T-branch and the non-excitation-side antenna, and they both couple the excitation-side antenna. As for the isolation of the antenna, it is improved by the offset of this interaction. Therefore, S_{12} has a significant reduction at most frequency bands, and at the same time, it can be seen from Fig. 4(a) that the increase in the T-shaped structure shifts the low-frequency band to the right and the high-frequency band to the left.

Referring to Fig. 3(c), to further improve the isolation and make the antenna operating band closer to that required for 5G and to generate a new band for future 6G, a ground-opening I-slit is cut below the T-branch, as the latter changes the current distribution of the ground transmission line through the I-slit and suppresses the mutual coupling caused by the ground surface waves, thus further improving the antenna isolation. At the same time, L-shaped radiating branches are added at both edges of the ground, and the loading of the L-shaped radiating branches changes the current flow path of the antenna to obtain better impedance matching. As shown in Fig. 3(d), the decoupling section is symmetrically distributed, and the I-slit operation is performed above the T-branch section, which changes the distribution parameters of the transmission line. Accordingly, the performance is improved by creating a slot in the ground plane. The slot functions as a resonator to obtain an additional resonant mode, where L_{s3} is the total length of the I-slot, and the resonant frequency f_{s3} is calculated to be 7.0 GHz.

$$L_{s3} = L_2 + L_7 \tag{5}$$

$$f_{s3} = \frac{c}{L_{s3}\sqrt{\varepsilon_\gamma}} \tag{6}$$

The final form of the fence-shaped structure is new, and it can help the antenna achieve better results. Hence, referring to Fig. 4(a), a new frequency band is created, the low-frequency band shifted to the right, and the high-frequency band shifted to the left, which is closer to the required frequency band for 5G. The final impedance bandwidths of the antenna are 3.37–3.6 GHz, 4.76–5.15 GHz, and 6.22–7.27 GHz, respectively, referring to Fig. 4(b), whereas the isolation degree is 13.1 dB.

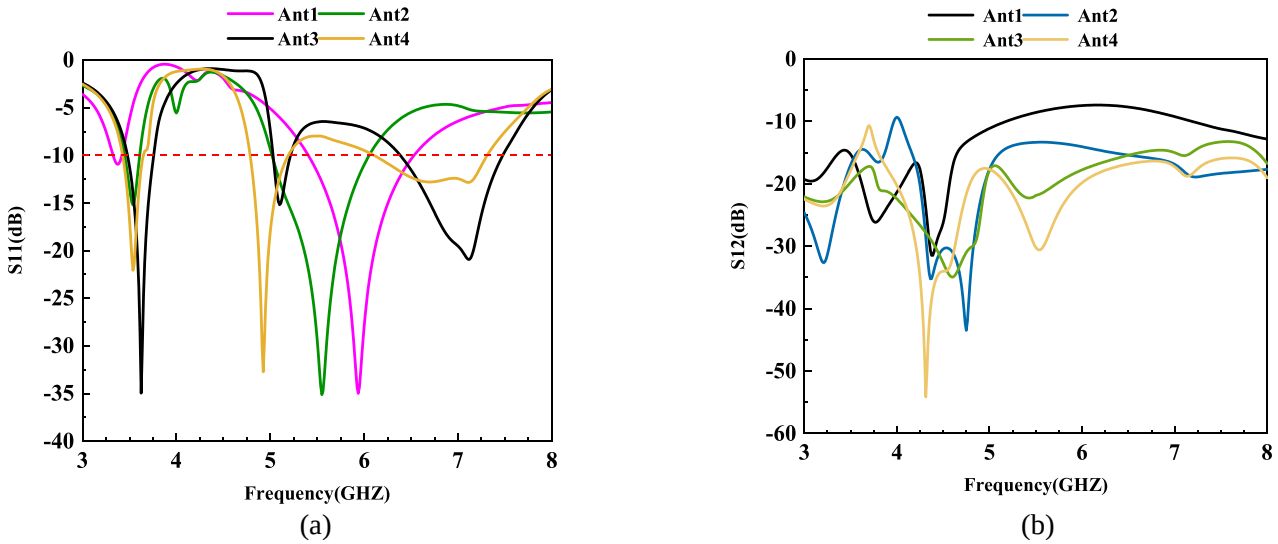

Figure 4. Simulation of S parameters of 4 antenna structures (a) S_{11} and (b) S_{12}.

2.2.2. Antenna Parameter Analysis

To optimize the performance of the designed MIMO antenna, the antenna structure and parameters are simulated and optimized by HFSS in the antenna design process. The optimization process adopts the method of optimizing one parameter while keeping the rest unchanged, and the optimization results are shown in Fig. 5. From Figs. 5(a), (b), and (c), it can be seen that parameters L_1, L_2, and L_9 mainly affect the resonant frequency of the antenna. When L_1 and L_2 are increased, the resonant frequency at the middle and high frequencies does not change significantly, and the resonant frequency at the low frequencies gradually shifts to the left when the lengths of L_1 and L_2 are increased. When L_1 is 46 mm and L_2 19.5 mm, the low-frequency center frequency is 3.4 GHz, which is in line with the design expectation. When L_9 increases, the resonant frequency at low frequency and middle frequency shifts left; the resonant frequency at high frequency does not change obviously; and the S_{11} of the antenna at high frequency decreases with the decrease of L_9 length, which means that the decrease of L_9 can improve the impedance matching of the antenna at high frequency. Finally, when L_9 is 6.8 mm, the center frequency at low frequency is 3.4 GHz; the center frequency at middle frequency is 4.9 GHz; and the center frequency at high frequency is 7 GHz. In summary, the optimal result is 46 mm for L_1, 19.5 mm for L_2, and 6.8 mm for L_9, which can get the frequency range coverage of 3.37 GHz–3.60 GHz, 4.76 GHz–5.15 GHz, and 6.22 GHz–7.27 GHz.

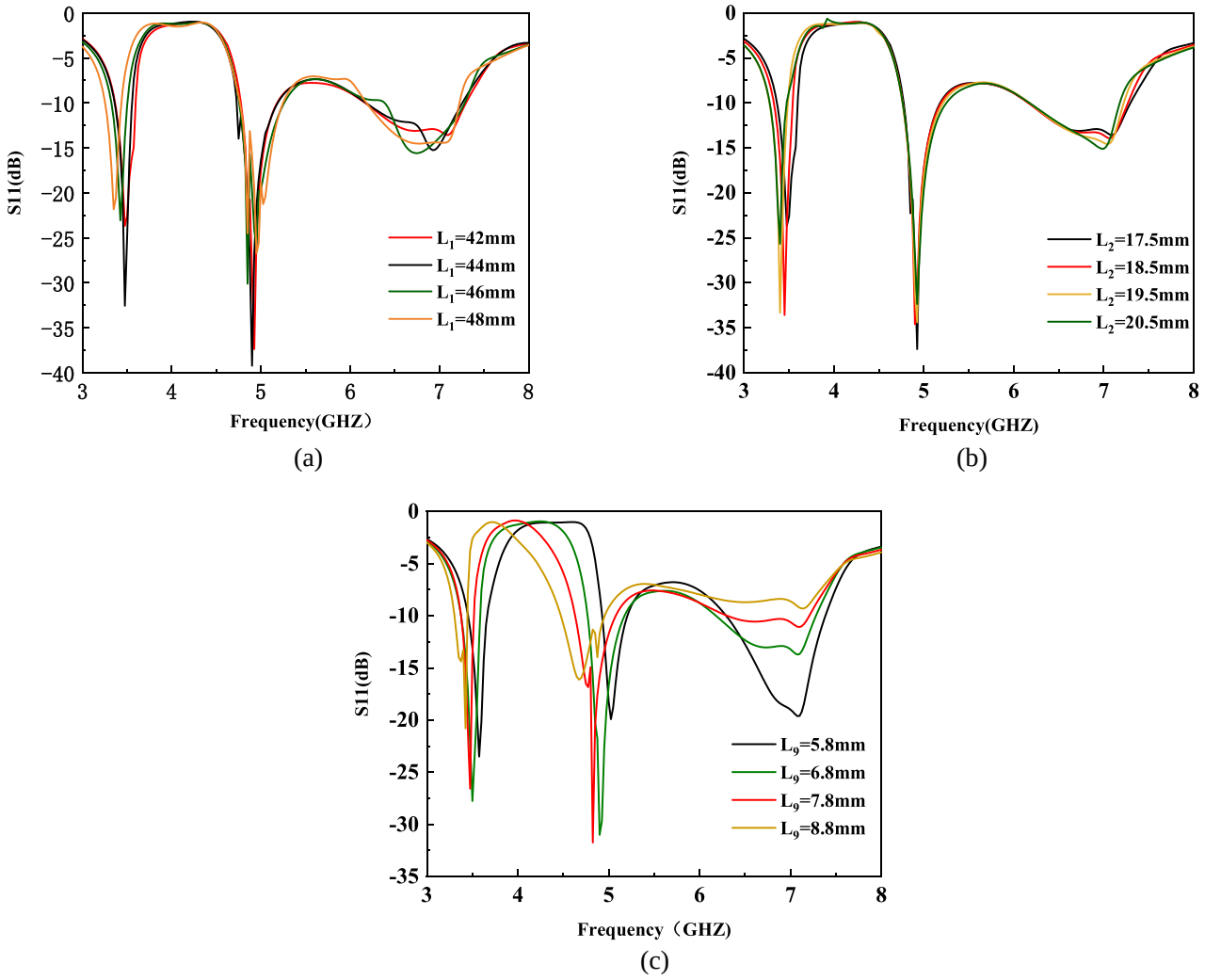

Figure 5. The effect of tuned parameters on S_{11} parameters (a) L_1, (b) L_2, and (c) L_9.

2.2.3. Antenna Surface Current Analysis

Figure 6 shows the surface current distribution of the modified MIMO antenna and further analyzes the effect of the change in the backplane section on the isolation of the antenna. Referring to Fig. 6(a), with the excitation of port 1, a large amount of current is coupled to port 2. Moreover, in Fig. 6(b), the introduction of the T-shaped ground plane reduces this coupling effect, whereas in Fig. 6(c), only a small amount of current is observed on the surface of the second antenna in the T-shaped ground plane. Finally, referring to Fig. 6(d), only a subtle amount of current is observed on the surface of the second antenna. Thus, the change in the geometric structure of the ground plane achieves a high level of isolation for the MIMO antenna. The absorption of the coupling current between the ports through the fence-shaped ground plane can be clearly observed, which effectively improves the port isolation between the two monopole antennas.

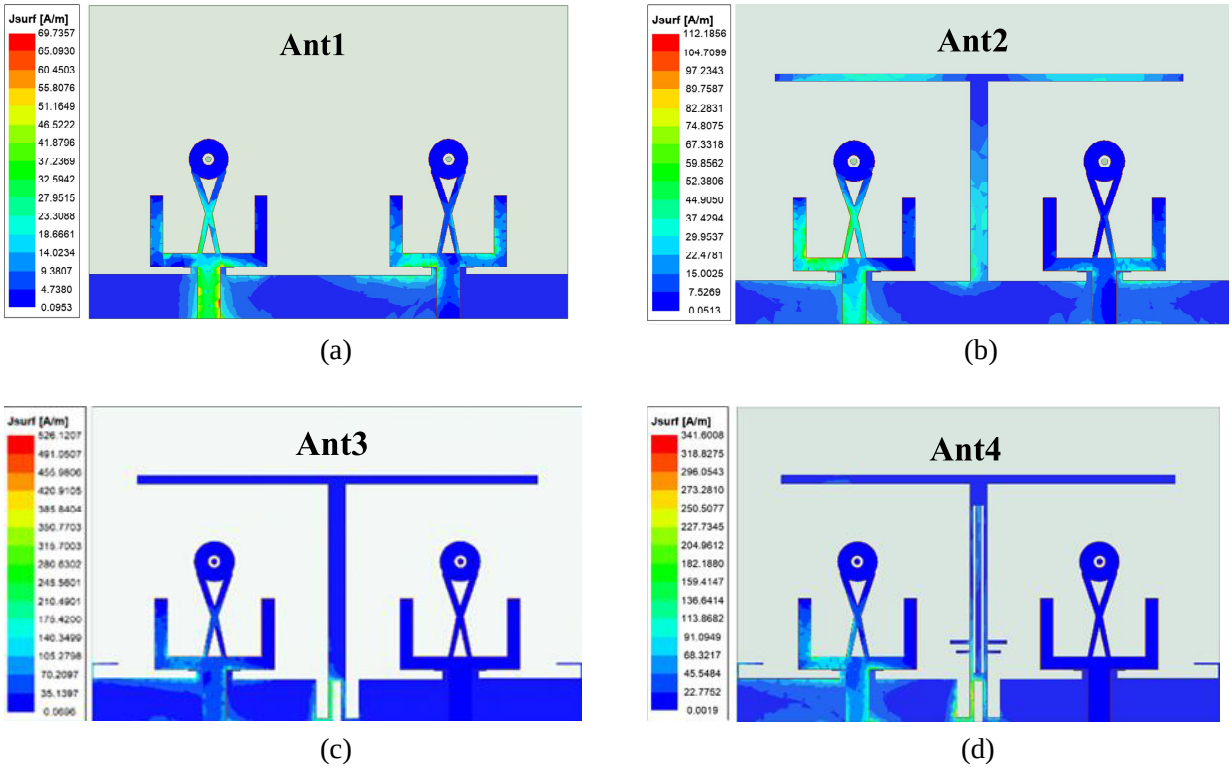

Figure 6. Comparison of surface current distributions of 4 antenna design steps (a) Ant1, (b) Ant2, (c) Ant3, and (d) Ant4.

3. EXPERIMENTAL SIMULATION AND MEASUREMENT

3.1. *S*-Parameters

S-parameters of the antenna are measured using an Agilent N5235A vector network analyzer. Fig. 7 shows the *S*-parameter measurement environment and the fabricated prototype. From the *S*-parameter curves in Fig. 8(a), the S_{11} measurement results of the antenna do not differ much from the simulated ones. The measured frequencies are a bit shifted to the left, but they still contain the required bandwidths of 3.38 GHz–3.61 GHz, 4.51 GHz–4.96 GHz, and 6.06 GHz–7.51 GHz. Moreover, errors may be caused by losses in the SMA connectors and transmission lines or by the test environment. Referring to the S_{12}-parameter curves shown in Fig. 8(b), the isolation degree of the antenna is more than 13 dB; therefore, the MIMO antenna achieves higher isolation between the two ports.

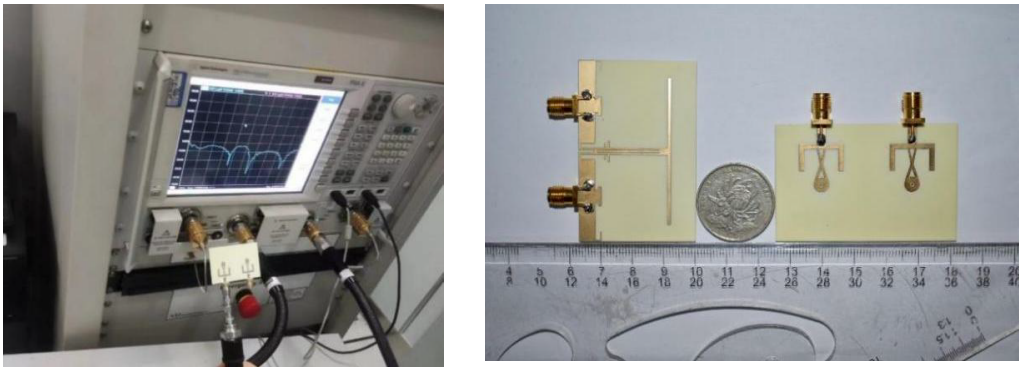

(a) (b)

Figure 7. The proposed antenna (a) S-parameters measurement environment and (b) fabricated prototype.

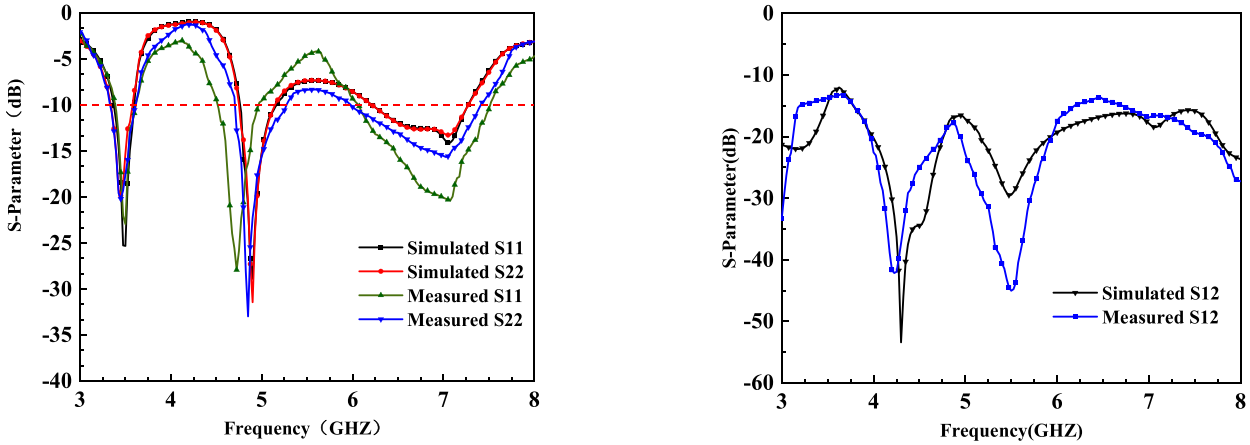

(a) (b)

Figure 8. Simulated and measured S parameters of the MIMO antenna: (a) S_{11} and (b) S_{12}.

3.2. Radiation Properties

The two-dimensional radiation direction maps of Port 1 measured on the E and H planes at 3.4 GHz, 4.9 GHz, and 7 GHz for MIMO antennas are represented in Fig. 9. It can be seen that, at a low frequency of 3.4 GHz, the radiation pattern of the antenna shows eight radiation characteristics in both the E-plane and H-plane, and the maximum radiation direction in the H-plane is distributed in 0–120 degrees and 180–300 degrees, whereas the maximum radiation direction in the E-plane is about 240 degrees and 105 degrees, which shows good radiation characteristics. At 4.9 GHz, the E surface shows almost omnidirectional radiation characteristics, and the radiation patterns of the H surface show a butterfly shape, in which the maximum radiation direction distribution ranges in 0–90 degrees and 150–240 degrees. As for the higher frequency of 7 GHz, the E surface shows an elliptical shape, reaching almost omnidirectional radiation characteristics; however, the direction of the H surface has been distorted, in the shape of flowers, where, at 105 degrees, 195 degrees, and 315 degrees, the radiation gain is more prominent, showing a stronger directional radiation performance. In general, the antenna has good radiation performance and a high gain at each frequency point, and the MIMO antenna is good for receiving and transmitting signals in all directions, thus realizing good radiation performance.

Figure 10 shows the results of the peak gain and the radiation efficiency of the antenna in the operating band. The peak gain of the antenna is about 1.5–6.5 dBi. In addition, the antenna has a high radiation efficiency in the frequency band, which exceeds 60%.

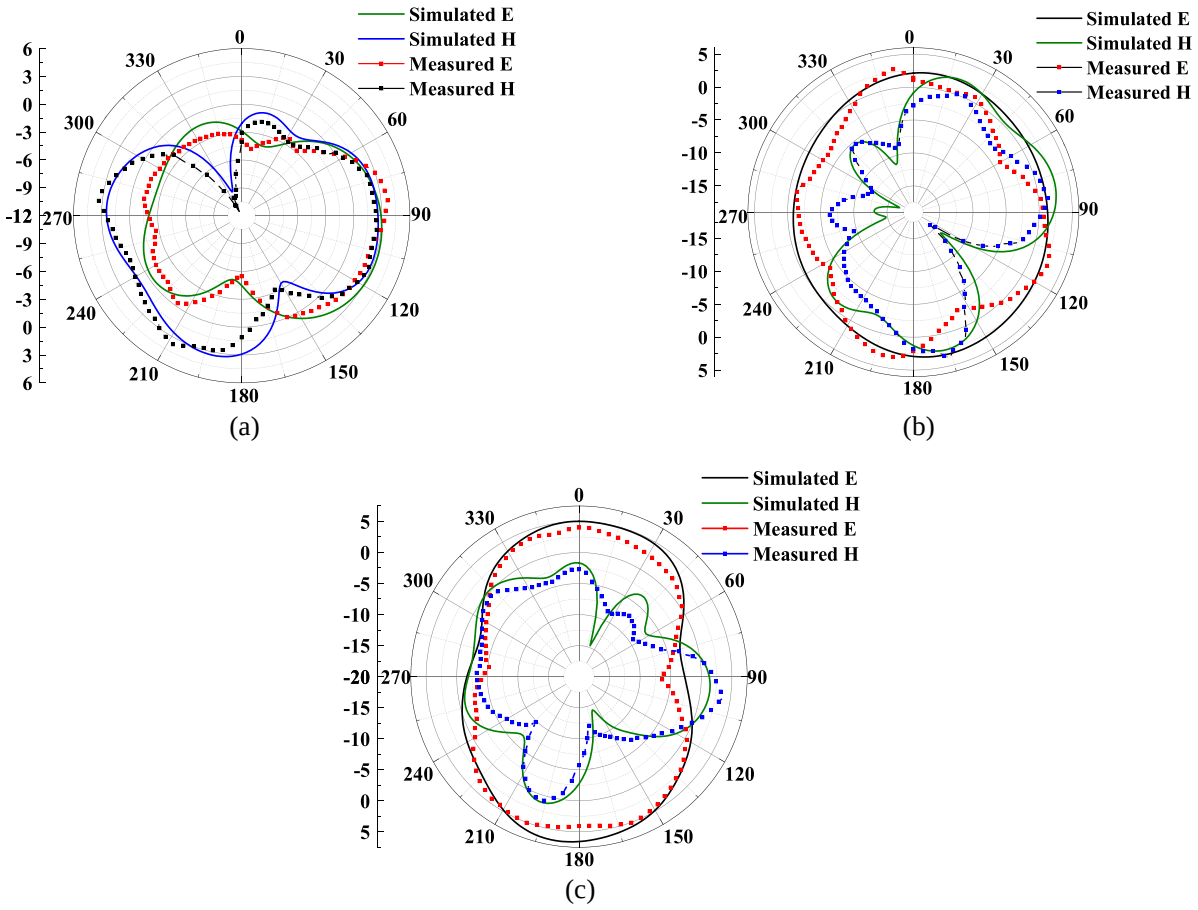

Figure 9. The simulated and measured radiation patterns at (a) 3.4 GHz, (b) 4.9 GHz, and (c) 7.0 GHz.

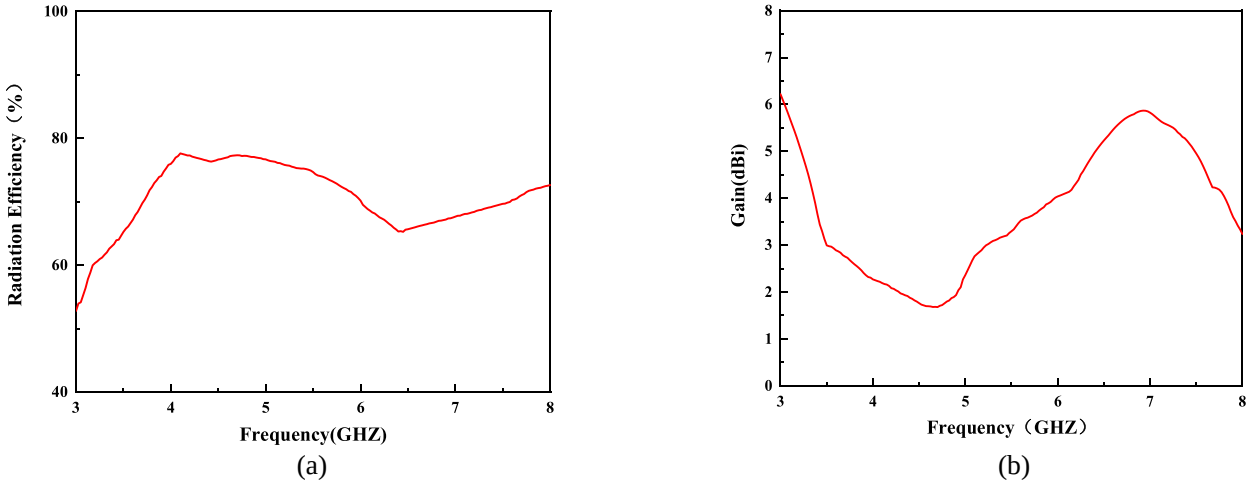

Figure 10. The proposed antenna: (a) radiation efficiency and (b) peak gain.

3.3. MIMO Diversity Performance

3.3.1. ECC

To ensure channel correlation in MIMO communication, the envelope correlation coefficient (ECC), a crucial MIMO performance statistic, is utilized to quantify the antenna diversity performance.

According to the regulations, the MIMO antenna elements must meet the ECC < 0.5 standards to achieve higher diversity between MIMO antenna elements [5]. For two-port MIMO antennas, the ECC is calculated using the following equation:

$$\mathrm{ECC} = \frac{|S_{12}^{*}S_{12} + S_{21}^{*}S_{22}|^{2}}{(1 - |S_{11}|^{2} - |S_{21}|^{2})\,(1 - |S_{22}|^{2} - |S_{12}|^{2})} \tag{7}$$

Moreover, the ECC value of the antenna is shown in Fig. 11 where it is below 0.2 in the frequency band, which meets the standard.

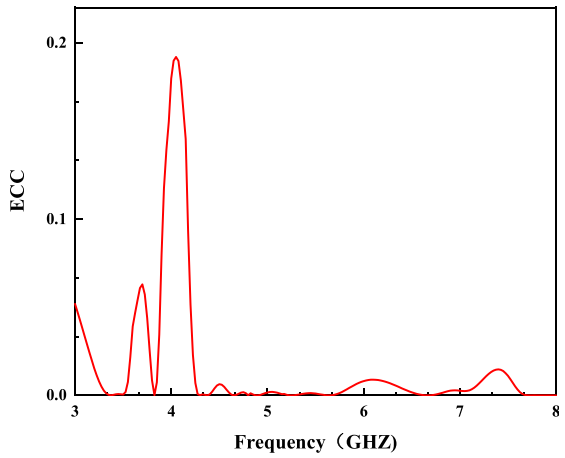

Figure 11. Envelope correlation coefficient of the antenna.

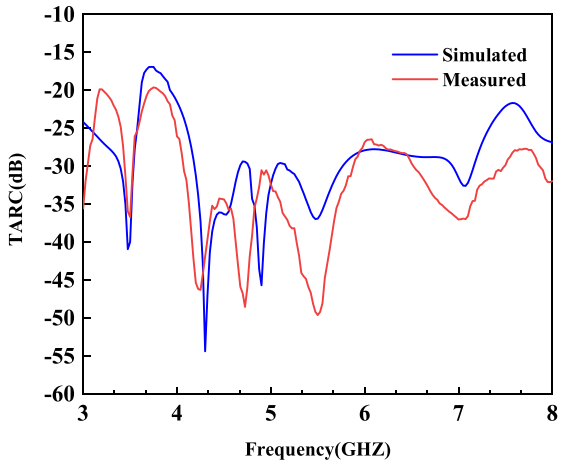

Figure 12. The TARC of the MIMO antenna.

3.3.2. TARC

The Total Active Reflection Coefficient (TARC), a new metric, is introduced as, for a multi-port antenna system, the adjacent antenna units influence each other, and the overall operating bandwidth and efficiency during operation are also affected, making the S-parameter alone insufficient to predict the actual system behavior. Therefore, the following equation can be used to determine the TARC of a two-port MIMO system:

$$\mathrm{TARC} = \sqrt{\frac{(S_{11} + S_{12})^{2} + (S_{21} + S_{22})^{2}}{2}} \tag{8}$$

For a MIMO system, a TARC < 0 dB is reasonable. Thus, Fig. 12 shows the TARC of the antenna. This value is smaller than -15 dB in the studied range, indicating that the MIMO coupling effect is low, and the lower TARC can ensure the independence of the different channels at the transmitter and receiver of the MIMO system, which can effectively exploit the effect of multipath to increase the system capacity.

3.4. Comparative Study

The proposed compact multiband antenna is comprehensively compared to several previously reported antennas in Table 2 in terms of size, isolation, operating frequency, radiation efficiency, and ECC. The proposed antenna has more available frequency bands than other works in the literature [13, 24–31]. Moreover, the decoupled structure of the proposed antenna is novel compared to [26–28]. Furthermore, the radiation efficiency in this work is better than [30, 31], and it has a smaller size than [27, 28]. Of course, the proposed MIMO system has good diversity and gain characteristics. To sum up, with comparable antenna performances, this antenna has a better performance and is well-suited for mobile terminals in various wireless communication networks. Table 2 shows a performance comparison of the proposed MIMO antenna with other works.

Table 2. Performance comparison of the proposed MIMO antenna with other works.

Ref.	Size (mm × mm × mm)	Operating frequency (GHz)	Isolation	Radiation Efficiency (%)	ECC
This work	56.4 × 36.6 × 1.524	3.37–3.6, 4.76–5.15, 6.22–7.27	> 13	> 50	< 0.2
[13]	150 × 75 × 0.8	3.3–3.84, 4.61–5.91	> 15	> 70	< 0.02
[24]	48.5 × 60.6 × 20	3.68–3.71, 4.08–4.13	> 20	> 95	< 0.01
[25]	70 × 70 × 0.8	2.3–2.5, 5.7–5.9	> 20	> 95	< 0.025
[26]	60 × 7.5 × 4.5	2.4–2.484, 5.15–5.85	> 16	> 95	-
[27]	96 × 65 × 0.2	3.05–3.74	> 15	> 95	< 0.1
[28]	52 × 77.5 × 1.6	2.4–2.48, 5.15–5.825	> 10	> 80	< 0.2
[29]	150 × 72 × 1.2	4.3–5.5	> 22	> 50	< 0.068
[30]	150 × 75 × 7	3.4–3.93, 4.5–5.3	> 10	> 50	< 0.23
[31]	32 × 20 × 0.8	3.3–7.8, 8–12	> 20	> 69	< 0.05

4. CONCLUSION

In this paper, a tri-band MIMO antenna, with high isolation, is designed for the 5G band and future 6G. Tri-band characteristics are promoted through a symmetric torch-shaped monopole antenna with a fence-shaped backplane structure covering the 5G bands at 3.4 GHz, 4.9 GHz, and the future 6 GHz band. The decreased decoupling between the dual ports is achieved by loading a fence-type structure, composed of a modified I-shaped ground slit and a T-shaped structure with symmetric L-shaped rectangular branches, which absorbs the ground currents. Finally, the dual-port MIMO antenna has a compact structure, small size, high radiation efficiency, and an acceptable ECC. From the above results, the proposed antenna is suitable for 5G and 6G communication.

ACKNOWLEDGMENT

This work was supported in part by the Anhui Provincial Natural Science Foundation under Grant No. 2108085MF200, in part by the Natural Science Research Project of Anhui Educational Committee under No. 2022AH051583 and No. 2022AH052138.

REFERENCES

1. Yuan, X. T., Z. Chen, T. Gu, and T. Yuan, "A wide band PIFA-pair-based MIMO antenna for 5G smartphones," *IEEE Antennas and Wireless Propagation Letters*, Vol. 20, No. 3, 371–375, 2021.
2. Pandya, A., T. K. Upadhyaya, and K. Pandya, "Tri-band defected ground plane based planar monopole antenna for Wi-Fi/WiMAX/WLAN applications," *Progress In Electromagnetics Research C*, Vol. 108, 127–136, 2021.
3. Kumar, N. R., P. D. Sathya, S. K. A. Rahim, et al., "Compact tri-band microstrip patch antenna using complementary split ring resonator structure," *Applied Computational Electromagnetics Society (ACES) Journal*, Vol. 36, No. 3, 346–353, 2021.
4. Mallat, N. K. and A. Iqbal, "Multi-band printed antenna for portable wireless communication applications," *Progress In Electromagnetics Research Letters*, Vol. 84, 39–46, 2019.

5. Singh, P. P. and S. K. Sharma, "Design and fabrication of a triple band microstrip antenna for WLAN, satellite TV and radar applications," *Progress In Electromagnetics Research C*, Vol. 117, 277–289, 2022.
6. Du, C., Z. Zhao, X. Wang, and F.-H. Yang, "A compact CPW-fed triple-band MIMO antenna with neutralization line decoupling for WLAN/WiMAX/5G applications," *Progress In Electromagnetics Research M*, Vol. 103, 129–140, 2021.
7. Iqbal, A., O. A. Saraereh, A. W. Ahmad, and S. Bashir, "Mutual coupling reduction using F-shaped stubs in UWB-MIMO antenna," *IEEE Access*, Vol. 6, 2755–2759, 2018.
8. Kumar, A., A. Q. Ansari, B. K. Kanaujia, J. Kishor, and S. Kumar, "An ultra-compact two-port UWB-MIMO antenna with dual band-notched characteristics," *AEU-International Journal of Electronics and Communications*, Vol. 114, 152997, 2020.
9. Masoodi, I., I. Ishteyaq, K. Muzaffar, and M. Magray, "A compact band-notched antenna with high isolation for UWB MIMO applications," *International Journal of Microwave and Wireless Technologies*, Vol. 13, No. 6, 634–640, 2021.
10. Deng, J. Y., J. Y. Li, L. Y. Zhao, et al., "A dua-L band in verted-F MIMO antenna with enhanced isolation for WLAN applications," *IEEE Antennas and Wireless Propagation Letters*, Vol. 16, 2270–2273, 2017.
11. Elfergani, I. T. E., A. S. Hussaini, R. A. Abd-Alhameed, C. H. See, M. B. Child, and J. Rodriguez, "Design of a compact tuned antenna system for mobile MIMO applications," *2012 Loughborough Antennas & Propagation Conference (LAPC)*, 1–4, Loughborough, UK, 2012.
12. Tan, X., W. Wang, Y. Wu, et al., "Enhancing isolation in dua-L band meander-line multiple antenna by employing split EBG structure," *IEEE Transactions on Antennas and Propagation*, Vol. 67, No. 4, 2769–2774, 2019.
13. Huang, J., G. Dong, Q. Cai, Z. Chen, L. Li, and G. Liu, "Dual-band MIMO antenna for 5G/WLAN mobile terminals," *Micromachines*, Vol. 12, No. 489, 1–12, 2021.
14. Gurjar, R., D. K. Upadhyay, B. K. Kanaujia, and A. Kumar, "A compact modified Sierpinski carpet fractal UWB MIMO antenna with square-shaped funnel-like ground stub," *AEU-International Journal of Electronics and Communications*, Vol. 117, 153–126, 2020.
15. Ahmad, S., S. Khan, B. Manzoor, M. Soruri, et al., "A compact CPW-fed ultra-wideband Multi-Input-Multi-Output (MIMO) antenna for wireless communication networks," *IEEE Access*, Vol. 10, 25278–25289, 2022.
16. Moradi, N., F. Nazari, H. Aliakbarian, and F. A. Namin, "Compact ultrawideband monopole antenna with continuously tunable notch band characteristics," *Progress In Electromagnetics Research C*, Vol. 118, 71–81, 2022.
17. Li, Y., C. Y. D. Sim, Y. Luo, and G. Yang, "High isolation 3.5 GHz eight-antenna MIMO array using balanced open-slot antenna element for 5G smartphones," *IEEE Transactions on Antennas and Propagation*, Vol. 67, No. 6, 3820–3830, 2019.
18. Yuan, X. T., Z. Chen, T. Gu, and T. Yuan, "A wideband PIFA-pair-based MIMO antenna for 5G smartphones," *IEEE Antennas and Wireless Propagation Letters*, Vol. 20, No. 3, 371–375, 2021.
19. Kumar, N. R., P. D. Sathya, S. K. A. Rahim, M. Z. M. Nor, A. Alomainy, and A. A. Eteng, "Compact tri-band microstrip patch antenna using complementary split ring resonator structure," *Applied Computational Electromagnetics Society (ACES) Journal*, Vol. 36, No. 3, 346–353, 2021.
20. Prabhu, P. and S. Malarvizhi, "Compact dual-band hybrid-fractal MIMO system for UMTS and LTE mobile applications," *Applied Computational Electromagnetics Society (ACES) Journal*, Vol. 34, No. 1, 135–140, 2019.
21. Yahya, L. S., L. S. Yahya, and K. H. Sayidmarie, "Dual-band folded monopole MIMO antennas with enhanced isolation," *Applied Computational Electromagnetics Society (ACES) Journal*, Vol. 36, No. 12, 1569–1578, 2021.
22. Li, Y., C. Y. D. Sim, Y. Luo, and G. Yang, "High isolation 3.5 GHz eight-antenna MIMO array using balanced open-slot antenna element for 5G smartphones," *IEEE Transactions on Antennas and Propagation*, Vol. 67, No. 6, 3820–3830, 2019.

23. Sharma, N. and S. S. Bhatia, "Metamaterial inspired fidget spinner-shaped antenna based on parasitic split ring resonator for multi-standard wireless applications," *Journal of Electromagnetic Waves and Applications*, Vol. 34, No. 10, 1471–1490, 2019.
24. Niu, Z., H. Zhang, Q. Chen, and T. Zhong, "Isolation enhancement in closely coupled dual-band MIMO patch antennas," *IEEE Antennas and Wireless Propagation Letters*, Vol. 18, No. 8, 1686–1690, Jul. 2019.
25. Shen, X., F. Liu, L. Zhao, G. L. Huang, X. Shi, Q. Huang, and A. Chen, "Decoupling of two strongly coupled dual-band antennas with reactively loaded dummy element array," *IEEE Access*, Vol. 7, 154672–154682, Oct. 2019.
26. Chou, J. H., J. F. Chang, D. B. Lin, and T. L. Wu, "Dual-band WLAN MIMO antenna with a decoupling element for full-metallic bottom cover tablet computer applications," *Microwave and Optical Technology Letters*, Vol. 60, No. 5, 1245–1251, May 2018.
27. Kulkarni, N., R. M. Linus, and N. B. Bahadure, "A small wideband inverted L-shaped flexible antenna for sub-6 GHz 5G applications," *AEU-International Journal of Electronics and Communications*, Vol. 159, 154479, 2023.
28. Deng, J., J. Li, L. Zhao, and L. Guo, "A dual-band inbacked-F MIMO antenna with enhanced isolation for WLAN applications," *IEEE Antennas and Wireless Propagation Letters*, Vol. 16, 2270–2273, 2017.
29. Cheng, B. and Z. Du, "Dual polarization MIMO antenna for 5G mobile phone applications," *IEEE Transactions on Antennas and Propagation*, Vol. 69, No. 7, 4160–4165, Jul. 2021.
30. Chen, Z., Y. Liu, T. Yuan, and H. Wong, "A miniaturized MIMO antenna with dual-band for 5G smartphone application," *IEEE Open Journal of Antennas and Propagation*, Vol. 4, 111–117, 2023.
31. Alharbi, G., J. Kulkarni, A. Desai, C. Y. D. Sim, and A. Poddar, "A multi-slot two antenna MIMO with high isolation for sub-6 GHz 5G/IEEE802.11ac/ax/C-band/X-band wireless and satellite applications," *Electronics*, Vol. 11, No. 3, 473, 2022.